Surface tension of the two center Lennard-Jones plus quadrupole model fluid

Stephan Werth, Martin Horsch[1], Hans Hasse

Laboratory of Engineering Thermodynamics, Department of Mechanical and Process Engineering, University of Kaiserslautern, Erwin-Schrödinger-Str. 44, 67663 Kaiserslautern, Germany

Abstract

The surface tension is determined by molecular dynamics simulation for the class of fluid models containing two Lennard-Jones centers and a point quadrupole (2CLJQ). The simulations are carried out with a long range correction for elongated molecules at planar interfaces, along the whole vapor pressure curve. The model parameters are varied systematically, covering the parameter range of 2CLJQ models for real fluids from the literature. Vapor-liquid equilibrium properties are obtained which agree well with literature data for 2CLJQ models. An empirical correlation for the surface tension is developed as a global function of the model parameters.

Keywords: Surface tension, Lennard-Jones potential, Quadrupole

1. Introduction

The two center Lennard-Jones plus quadrupole (2CLJQ) class of molecular models provides a straightforward description of the intermolecular in-

[1]Author to whom correspondence should be addressed: martin.horsch@mv.uni-kl.de.

teraction in many compounds such as air components [1–7], halogens [1, 8], refrigerants [9] and hydrocarbons [1]. For example, various 2CLJQ molecular models exist for carbon dioxide [1–3], nitrogen [1, 4–7], oxygen [1, 7] and chlorine [1, 8]. Table 1 shows an overview of 2CLJQ molecular models for real fluids from the literature.

[Table 1 about here.]

These molecular models are usually adjusted to bulk properties of vapor-liquid equilibria [1–3, 6, 9] like the vapor pressure, the enthalpy of vaporization and saturated densities, or the second virial coefficient [3]. The surface tension of these molecular models was up to now not taken into account in the parameterization. Nonetheless, the surface tension of 2CLJQ nitrogen and oxygen models adjusted to vapor-liquid equilibrium bulk properties is known to agree well with experimental data [10, 11]. However, a systematic study on the surface tension of 2CLJQ models has not been conducted so far. The present work closes this gap, providing detailed information on the relation between 2CLJQ model parameters and the surface tension obtained by molecular simulation. It can, e.g., be used for adjusting model parameters to surface tension data.

In molecular simulation, bulk properties of fluid phases in thermodynamic equilibrium can be computed by various methods, like Grand Equilibrium [12], NpT plus test particle simulation [13], or the Gibbs ensemble method [14]. The computation of interfacial properties is not possible with these methods as no interface is present. Instead, a single simulation volume containing the liquid and the vapor phase, separated by an interface,

is needed. Directly sampling the interface has the consequence that because of the heterogeneity of the system, the long range contribution of the interaction potential becomes more significant [15–17]. However, for numerical reasons the interaction potential has to be cut off. The error made by this simplification is accounted for by an asymmetrical long range correction, which can be based on fast multipole methods [18, 19], slab based tail corrections [15, 20, 21] or Ewald summation techniques [22, 23]. Even though these methods differ considerably in their algorithms, the results in terms of the saturated liquid density and the surface tension in systems with multiple Lennard-Jones sites of the most recent versions of these approaches are similar [20, 23].

In previous work, vapor-liquid equilibria of the 2CLJQ fluid were examined and correlated [1, 9, 24]. Additionally, transport properties of the 2CLJQ fluid were determined for model fluids [25] as well as 2CLJQ molecular models describing real fluid behavior [26, 27]. In the present work, the surface tension of the 2CLJQ model fluid is determined and a correlation for the simulation data is given. These results can be used for the optimization of molecular models.

2. Simulation

The molecular models considered in the present work consist of two identical Lennard-Jones sites, which are at a distance L apart from each other, and a point quadrupole in the center of mass. The Lennard-Jones potential is described by

$$u_{ij}^{\mathrm{LJ}} = 4\epsilon \left[\left(\frac{\sigma}{r_{ij}} \right)^{12} - \left(\frac{\sigma}{r_{ij}} \right)^{6} \right], \tag{1}$$

with the energy parameter ϵ and the size parameter σ, where r_{ij} is the distance between the two interaction sites. The quadrupole-quadrupole interaction is described by

$$u_{ij}^{\mathrm{Q}} = \frac{1}{4\pi\epsilon_0}\frac{3}{4}\frac{Q_i Q_j}{r_{ij}^5} f(\omega), \tag{2}$$

where ϵ_0 is the electric constant, Q_i and Q_j are the quadrupole moments of the two molecules, and $f(\omega)$ is a dimensionless angle-dependent expression [28].

All thermodynamic properties are given here in terms of σ, ϵ and m, as well as the Boltzmann constant k_{B} and the Coulomb constant $1/4\pi\epsilon_0$, i.e.

$$\text{temperature } T = T^* \, \epsilon \, / \, k_{\mathrm{B}}, \tag{3}$$

$$\text{pressure } p = p^* \, \epsilon \, / \, \sigma^3, \tag{4}$$

$$\text{density } \rho = \rho^* \, / \, \sigma^3, \tag{5}$$

$$\text{surface tension } \gamma = \gamma^* \, \epsilon \, / \, \sigma^2. \tag{6}$$

This approach effectively reduces the number of parameters of the 2CLJQ model fluid to two: the reduced elongation $L^* = L \, / \, \sigma$ and the reduced squared quadrupole moment $Q^{*2} = Q^2 \, / \, (4\pi\epsilon_0 \, \epsilon \, \sigma^5)$. The simulation grid, containing the parameters of the simulated fluids, is shown in Figure 1, which also includes molecular models for real fluids from the literature [1–9]. Simulations were performed from 0.6 to 0.9 T_{c}^*, where $T_{\mathrm{c}}^*(Q^{*2}, L^*)$ is the critical temperature estimated by an equation of state for the 2CLJQ fluid [24]. The liquid phase was situated in the center of the simulation volume and surrounded by vapor on both sides.

[Figure 1 about here.]

The surface tension γ was obtained from the difference between the normal and tangential contributions to the virial $\Pi_\mathrm{N} - \Pi_\mathrm{T}$, which is equivalent to the integral over the differential pressure $p_\mathrm{N} - p_\mathrm{T}$

$$\gamma = \frac{1}{2A} \left(\Pi_\mathrm{N} - \Pi_\mathrm{T} \right) = \frac{1}{2} \int_{-\infty}^{\infty} \mathrm{d}y \left(p_\mathrm{N} - p_\mathrm{T} \right) , \tag{7}$$

where $2A$ denotes the surface area of the two dividing surfaces in a simulation volume with periodic boundary conditions [21, 29].

A center-of-mass cutoff radius of 5 σ was used. Beyond the cutoff radius a slab-based long range correction (LRC) with angle averaging was used for the Lennard-Jones interactions [20], while the point quadrupole was assumed to have no preferred orientation beyond the cutoff radius, which yields a vanishing LRC contribution.

The simulations were performed with the $ls1$ *mardyn* molecular dynamics code [30, 31] in the canonical ensemble. A number of particles of $N = 16\ 000$ was used throughout. The equation of motion was solved by a leapfrog integrator [32] with a time step of $\Delta t^* = 0.001$. The elongation of the simulation volume normal to the interface was $l_y^* = 60$ and the thickness of the liquid film was $l_\mathrm{lf}^* = 30$, to minimize finite size effects [33]. The extension of the simulation volume in the other spatial directions was at least $l_\mathrm{x}^* = l_\mathrm{z}^* = 20$ to minimize the error due to truncating the capillary wave spectrum [34–37]. The equilibration was conducted for 500 000 time steps and the production runs for 2 500 000 time steps, so that highly precise simulation results were obtained (see below). The statistical errors were estimated to be the triple standard deviation of five block averages, each over 500 000 time steps. The saturated densities and the vapor pressures were calculated as an average over the respective phases excluding the interfacial region.

3. Results and Discussion

Table 2 shows the results for the saturated liquid density $\rho^{*'}$, the saturated vapor density $\rho^{*''}$, the vapor pressure p^{S*} and the surface tension γ^* obtained for the 30 considered parameter sets of the 2CLJQ model class.

[Table 2 about here.]

Stoll et al. [24] used the Grand Equilibrium method for the determination of the vapor-liquid equilibria of 2CLJQ model fluids. Figures 2 and 3 show the correlations for the saturated densities and the vapor pressure curve from Stoll et al. [24] in comparison to the simulation results from the present work. The deviation between the correlation and the simulation result is consistently smaller than the simulation error (except for a single value).

[Figure 2 about here.]

[Figure 3 about here.]

The results for the surface tension of the 2CLJQ model fluids are shown in Figure 4 for three different elongations and three different quadrupole moments.

[Figure 4 about here.]

Correlations for the surface tension are usually given in the form

$$\gamma = A \left(1 - \frac{T}{T_c}\right)^B , \tag{8}$$

which is also used here. In agreement with the theory of universal critical scaling, a constant value of B is employed here for the correlation expression.

The critical temperature T_c^* is calculated with the correlation of Stoll et al. [24], and $A^*\left(Q^{*2}, L^*\right)$ is fitted adopting the approach of Stoll et al. [24]

$$A^*\left(Q^{*2}, L^*\right) = a_1 + \sum_{i=1}^{3} b_i Q^{*2i} + c_1 / \left(L^{*2} + 0.1\right) + \sum_{i=2}^{3} d_i Q^{*4} L^{*i} + \sum_{i\in\{2,5\}} e_i Q^{*4} / \left(L^{*i} + 0.1\right). \quad (9)$$

Fitting the parameters of Eq. (9) as well as the B parameter from Eq. (8) simultaneously to the simulation results yields the exponent $B = 1.2378$, which is similar to exponents found for the pure Lennard-Jones fluid [33]. The remaining parameters of Eq. (9) are shown in Table 3. The correlation generally agrees with the simulation data within their statistical uncertainties, cf. Figures 4 and 5. The relative deviation between the simulation data and the correlation, cf. Figure 5, increases at higher temperatures due to fluctuations close to the critical point and the lower numerical value of the surface tension. The relative mean deviation between the simulation results and the correlation is 1.9 %.

[Figure 5 about here.]

[Table 3 about here.]

The correlation for the surface tension describes the increasing surface tension for larger quadrupole moments as well as the decrease of the surface tension with increasing elongation.

Figure 6 shows the surface tension of the 2CLJQ model fluids over the density difference between the saturated liquid density and the saturated

vapor density. The surface tension of a given substance only depends on the density difference [38, 39]

$$\gamma \propto \left(\rho' - \rho''\right)^{3B}. \tag{10}$$

According to Sugden [40], the prefactor for Eq. (10) is called the parachor P, leading to

$$\gamma = \left(P \frac{\rho' - \rho''}{m}\right)^{3B}, \tag{11}$$

where m is the molar mass. The reduced mass is $m^* = 2$ here, since the mass of the molecule is reduced by the mass of a single Lennard-Jones site. The parachor P is only a function of the elongation

$$P^*\left(L^*\right) = \alpha_1 + \sum_{i=1}^{3} \beta_i L^{*i}, \tag{12}$$

and the parameters of Eq. (12) are given in Table 4.

[Table 4 about here.]

Two major phenomena can be observed from the present simulations: An increase in the quadrupole moment leads to an increase in both the surface tension and the density difference, whereas increasing the elongation results in a smaller density difference, which reduces the surface tension. These effects are both well described by the parachor correlation given by Eq. (12). They can be exploited during the optimization of 2CLJQ molecular models for real fluids [41].

[Figure 6 about here.]

4. Conclusion

In the present work, the surface tension of 30 2CLJQ model fluids was computed by molecular dynamics simulation. A correlation for the surface tension in dependence of the parameters of the 2CLJQ model fluid was developed. The deviation between the correlation and simulation data is within the statistical uncertainties. The saturated densities and the vapor pressures agree with the results from Stoll et al. [24] within the statistical uncertainties as well. The correlation can be used to adjust 2CLJQ molecular models to the surface tension over the whole temperature range.

Acknowledgement

The authors gratefully acknowledge financial support from Deutsche Forschungsgemeinschaft (DFG) within the Collaborative Research Center (SFB) 926 as well as the German Federal Ministry of Education and Research (BMBF) within the SkaSim project, and they thank Jadran Vrabec and Katrin Stöbener for fruitful discussions. The present work was conducted under the auspices of the Boltzmann-Zuse Society of Computational Molecular Engineering (BZS), and the simulations were carried out on the *elwetritsch* cluster at the Regional University Computing Center Kaiserslautern (RHRK) under the grant TUKL-MSWS and on the *SuperMUC* supercomputer at Leibniz-Rechenzentrum Garching within the large-scale scientific computing project pr83ri.

[1] J. Vrabec, J. Stoll, and H. Hasse. *J. Phys. Chem. B*, 105(48):12126–12133, 2001.

[2] D. Möller and J. Fischer. *Fluid Phase Equilib.*, 100:35–61, 1994.

[3] C. S. Murthy, K. Singer, and I. R. McDonald. *Mol. Phys.*, 44(1):135–143, 1981.

[4] P. S. Y. Cheung and J. G. Powles. *Mol. Phys.*, 32(5):1383–1405, 1976.

[5] C. S. Murthy, K. Singer, M. I. Klein, and I. R. McDonald. *Mol. Phys.*, 41(6):1387–1399, 1980.

[6] C. Kriebel, A. Müller, M. Mecke, J. Winkelmann, and J. Fischer. *Int. J. Thermophys.*, 17(6):1349–1363, 1996.

[7] J.-P. Bouanich. *J. Quant. Spectrosc. Radiat. Transfer*, 47(4):243–250, 1991.

[8] C. S. Murthy, K. Singer, and R. Vallauri. *Mol. Phys.*, 49(4):803–815, 1983.

[9] J. Stoll, J. Vrabec, and H. Hasse. *J. Chem. Phys.*, 119(21):11396–11407, 2003.

[10] J.-C. Neyt, A. Wender, V. Lachet, and P. Malfreyt. *J. Phys. Chem. B*, 115(30):9421–9430, 2011.

[11] S. Eckelsbach, S. Miroshnichenko, G. Rutkai, and J. Vrabec. In W. E. Nagel, D. B. Kröner, and M. M. Resch, editors, *High Performance Computing in Science and Engineering '13*, pages 635–646. Springer, Berlin/Heidelberg, 2013.

[12] J. Vrabec and H. Hasse. *Mol. Phys.*, 100(21):3375–3383, 2002.

[13] D. Möller and J. Fischer. *Mol. Phys.*, 69(3):463–473, 1990.

[14] A. Z. Panagiotopoulos. *Mol. Phys.*, 61(4):813–826, 1987.

[15] M. Mecke, J. Winkelmann, and J. Fischer. *J. Chem. Phys.*, 107(21):9264–9270, 1997.

[16] J. Alejandre and G. A. Chapela. *J. Chem. Phys.*, 132:014701, 2010.

[17] K. F. Mansfield and D. M. Theodorou. *Macromolecules*, 24(15):4295–4309, 1991.

[18] G. Mathias, B. Egwolf, M. Nonella, and P. Tavan. *J. Chem. Phys.*, 118(24):10847–10860, 2003.

[19] R. Yokota, J. P. Badhan, M. G. Knepley, L. A. Barba, and T. Hamada. *Comp. Phys. Comm.*, 182(6):1272–1283, 2011.

[20] S. Werth, G. Rutkai, J. Vrabec, M. Horsch, and H. Hasse. *Mol. Phys.*, 112(17):2227–2234, 2014.

[21] J. Janeček. *J. Phys. Chem. B*, 110(12):6264–6269, 2006.

[22] P. J. in 't Veld, A. E. Ismail, and G. S. Grest. *J. Chem. Phys.*, 127:144711, 2007.

[23] R. E. Isele-Holder, W. Mitchell, and A. E. Ismail. *J. Chem. Phys.*, 137:174107, 2012.

[24] J. Stoll, J. Vrabec, H. Hasse, and J. Fischer. *Fluid Phase Equilib.*, 179:339–362, 2001.

[25] G. A. Fernández, J. Vrabec, and H. Hasse. *Fluid Phase Equilib.*, 249:120–130, 2006.

[26] G. A. Fernández, J. Vrabec, and H. Hasse. *Int. J. Thermophys.*, 26:1389–1407, 2005.

[27] G. A. Fernández, J. Vrabec, and H. Hasse. *Mol. Sim.*, 31(11):787–793, 2005.

[28] C. G. Gray and K. E. Gubbins. *Theory of Molecular Fluids, Vol. 1: Fundamentals*. Clarendon Press, Oxford, 1984.

[29] J. P. R. B. Walton, D. J. Tildesley, J. S. Rowlinson, and J. R. Henderson. *Mol. Phys.*, 48(6):1357–1368, 1983.

[30] M. Buchholz, H.-J. Bungartz, and J. Vrabec. *J. Computat. Sci.*, 2(2):124–129, 2011.

[31] C. Niethammer, S. Becker, M. Bernreuther, M. Buchholz, W. Eckhardt, A. Heinecke, S. Werth, H.-J. Bungartz, C. W. Glass, H. Hasse, J. Vrabec, and M. Horsch. *J. Chem. Theory Comput.*, 10(10):4455–4464, 2014.

[32] D. Fincham. *Mol. Phys.*, 8(3-5):165–178, 1992.

[33] S. Werth, S. V. Lishchuk, M. Horsch, and H. Hasse. *Physica A*, 392(10):2359–2367, 2013.

[34] P. Orea, J. López Lemus, and J. Alejandre. *J. Chem. Phys.*, 123:114702, 2005.

[35] G. J. Gloor, G. Jackson, F. J. Blas, and E. de Miguel. *J. Chem. Phys.*, 123:134703, 2005.

[36] A. Werner, F. Schmid, M. Müller, and K. Binder. *J. Chem. Phys.*, 107(19):8175–8188, 1997.

[37] J. Janeček. *J. Chem. Phys.*, 131:124513, 2009.

[38] D. B. Macleod. *Transact. Faraday Soc.*, 19:38–41, 1923.

[39] E. A. Guggenheim. *J. Chem. Phys.*, 13:253–261, 1945.

[40] S. Sugden. *J. Chem. Soc.*, 125:1177–1189, 1924.

[41] S. Werth, K. Stöbener, P. Klein, K.-H. Küfer, M. Horsch, and H. Hasse. *Chem. Eng. Sci.*, 121:110–117, 2015.

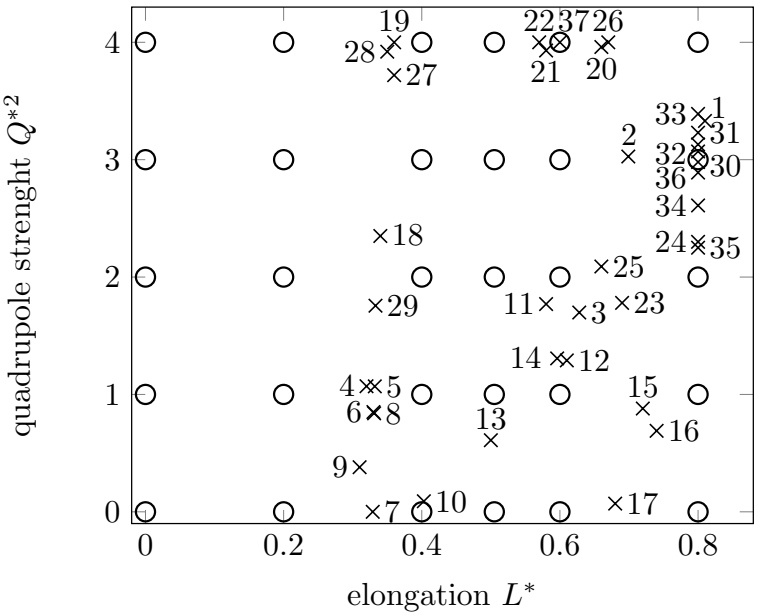

Figure 1: Reduced parameters of the simulated 2CLJQ model fluids. Open symbols denote the model fluids studied in the present work, crosses correspond to molecular models which represent real fluids. The numbers identify the real fluids and the authors given in Table 1.

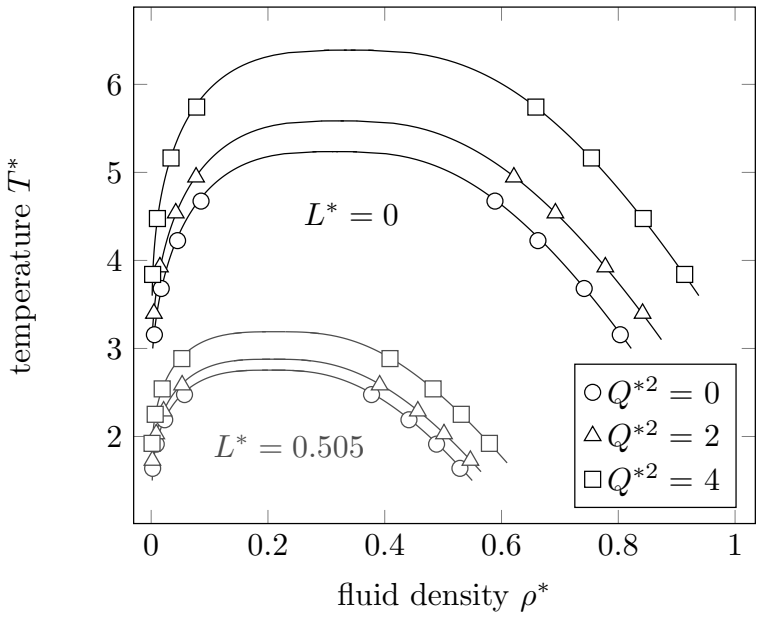

Figure 2: Saturated densities of the 2CLJQ model fluid. The symbols are the simulation results from the present work. The solid lines are correlations from Stoll et al. [24]. The simulation uncertainties are smaller than the symbol size in all cases.

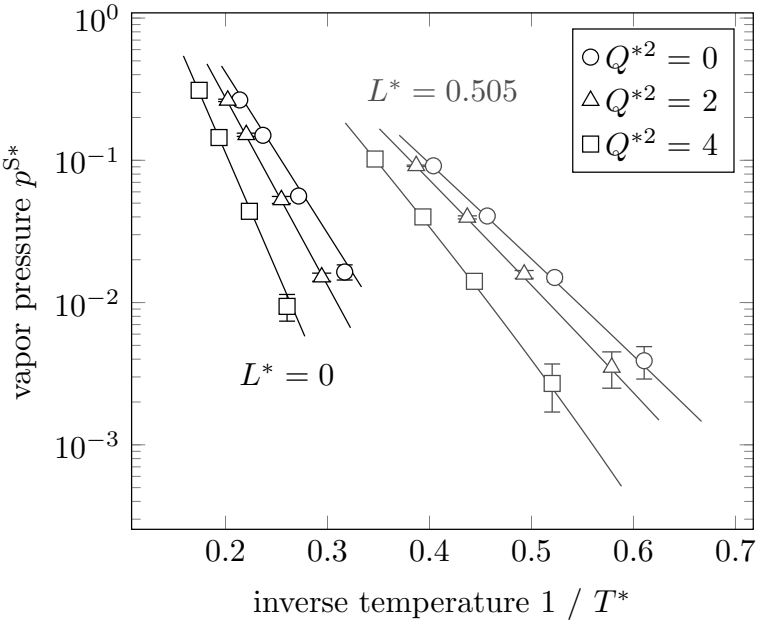

Figure 3: Vapor pressure curves of the 2CLJQ model fluid. The symbols are the simulation results from the present work. The solid lines are correlations from Stoll et al. [24].

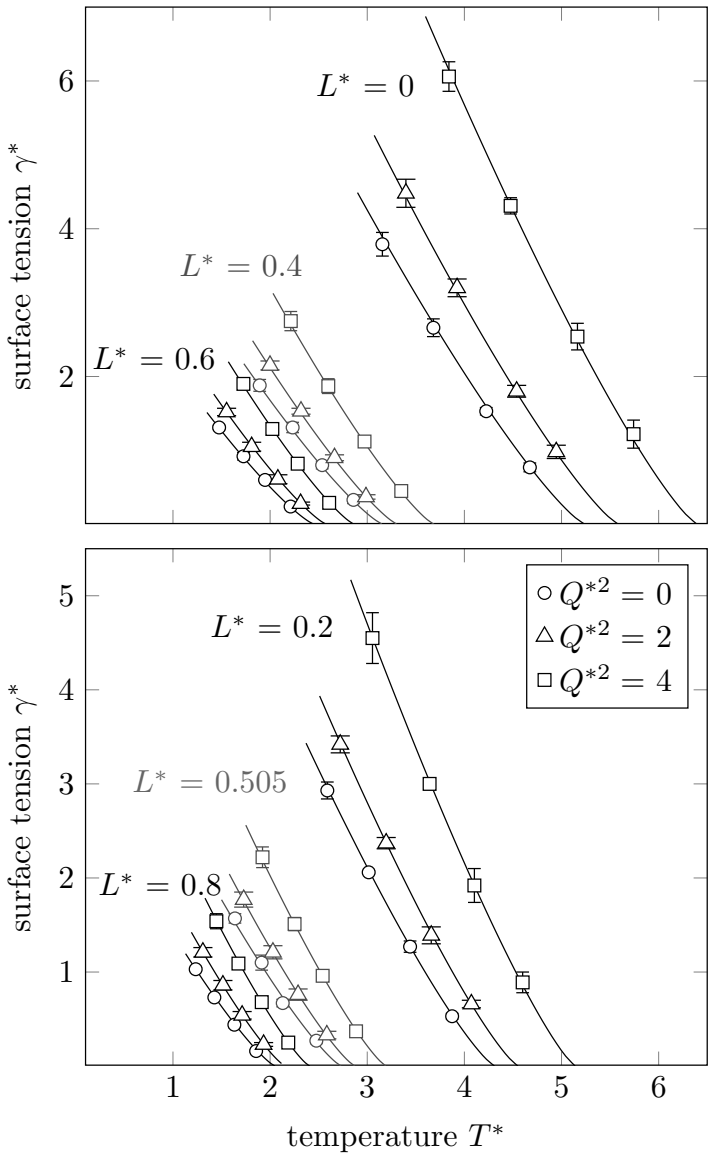

Figure 4: Surface tension of the 2CLJQ model fluid over the temperature. The solid line represents the correlation given in Eqs. (8) and (9).

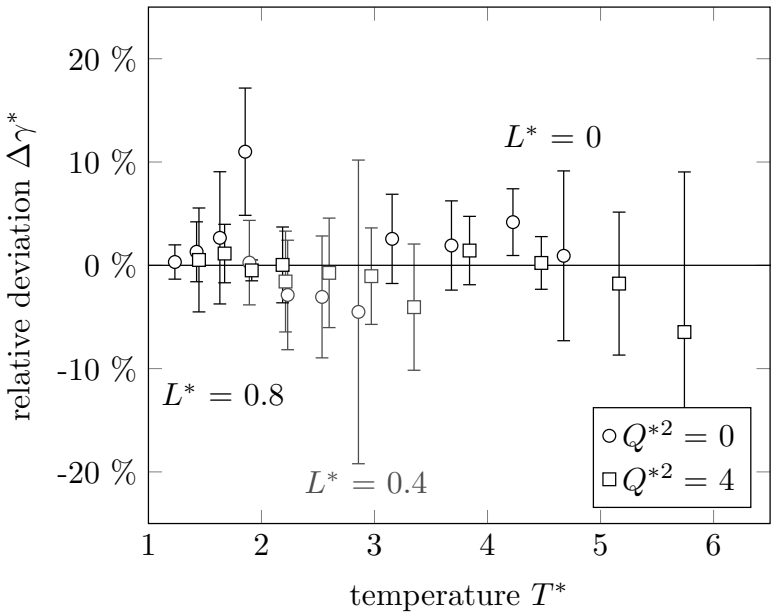

Figure 5: Relative deviations $\Delta\gamma^* = (\gamma^*_{\mathrm{corr}} - \gamma^*_{\mathrm{sim}}) \,/\, \gamma^*_{\mathrm{sim}}$ of simulation results for the surface tension of the 2CLJQ model fluid from the correlation given by Eqs. (8) and (9).

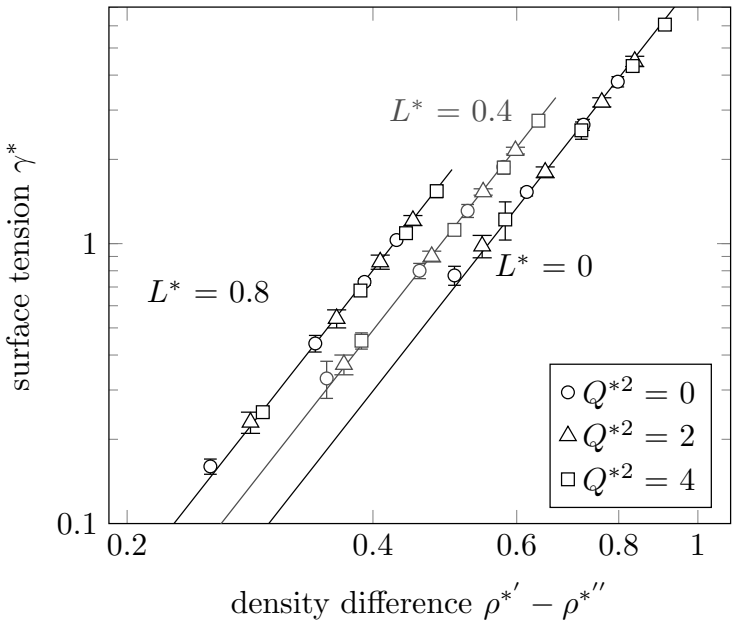

Figure 6: Surface tension of the 2CLJQ model fluid over the difference between the saturated liquid and the saturated vapor density. The solid line represents the correlation from Eqs. (12) for the respective elongation.

Table 1: Overview of 2CLJQ molecular models for real fluids from the literature. Numbers are used for identification, cf. Figure 1.

CO_2	1,2,3	C_2H_2	19	CO	29
N_2	4,5,6,7,8	C_2F_6	20	R113	30
O_2	9,10	C_2F_4	21	R114	31
Cl_2	11,12	C_2Cl_4	22	R115	32
F_2	13	Propadiene	23	R134	33
Br_2	14	Propyne	24	R30B2	34
I_2	15	Propylene	25	R150B2	35
CS_2	16	SF_6	26	R114B2	36
C_2H_6	17	CF_4	27	R1120	37
C_2H_4	18	CCl_4	28		

Vrabec et al. [1]	1,4,9,11,13,14,15,16,17,18,19, 20,21,22,23,24,25,26,27,28
Möller and Fischer [2]	2
Murthy et al. [3]	3
Cheung and Powles [4]	5
Murthy et al. [5]	6
Kriebel et al. [6]	7
Bouanich [7]	8,10
Murthy et al. [8]	12
Stoll et al. [9]	29,30,31,32,33,34,35,36,37

Table 2: Vapor-liquid equilibrium data for 2CLJQ model fluids. The numbers in parentheses indicate the uncertainties of the last decimal digits.

$L^* = 0$	T^*	p^{S*}	$\rho^{*'}$	$\rho^{*''}$	γ^*
$Q^{*2} = 0$	3.156	0.016(1)	0.8034(2)	0.0055(3)	3.79(16)
	3.681	0.056(2)	0.7416(2)	0.0172(8)	2.66(12)
	4.225	0.150(5)	0.6624(1)	0.0452(2)	1.53(5)
	4.674	0.266(3)	0.5888(7)	0.0854(18)	0.77(6)
$Q^{*2} = 1$	3.132	0.012(1)	0.8257(2)	0.0041(4)	4.22(5)
	3.712	0.051(2)	0.7571(2)	0.0153(7)	2.91(11)
	4.187	0.120(2)	0.6929(3)	0.0351(5)	1.89(9)
	4.773	0.273(2)	0.5927(11)	0.0856(9)	0.77(8)
$Q^{*2} = 2$	3.398	0.015(1)	0.8416(1)	0.0047(5)	4.48(19)
	3.925	0.053(3)	0.7778(2)	0.0150(8)	3.20(12)
	4.538	0.151(4)	0.6923(4)	0.0421(12)	1.80(8)
	4.946	0.264(5)	0.6212(6)	0.0769(19)	0.98(9)
$Q^{*2} = 3$	3.505	0.009(1)	0.8876(3)	0.0026(2)	5.45(15)
	4.106	0.041(1)	0.8178(1)	0.0111(3)	3.86(10)
	4.741	0.133(3)	0.7333(3)	0.0339(8)	2.30(6)
	5.341	0.302(8)	0.6319(9)	0.0826(3)	1.01(10)
$Q^{*2} = 4$	3.841	0.009(1)	0.9137(1)	0.0025(3)	6.06(20)
	4.476	0.044(4)	0.8427(3)	0.0107(9)	4.31(11)
	5.164	0.145(5)	0.7540(4)	0.0340(1)	2.54(18)
	5.742	0.311(5)	0.6588(19)	0.0779(16)	1.22(19)

$L^* = 0.2$	T^*	p^{S*}	$\rho^{*'}$	$\rho^{*''}$	γ^*
$Q^{*2} = 0$	2.589	0.011(1)	0.7108(1)	0.0044(5)	2.93(9)
	3.015	0.037(1)	0.6573(3)	0.0137(3)	2.06(2)
	3.441	0.095(2)	0.5955(4)	0.0345(11)	1.27(6)
	3.874	0.197(3)	0.5141(6)	0.0771(16)	0.53(3)
$Q^{*2} = 1$	2.625	0.010(1)	0.7206(1)	0.0040(3)	3.10(12)
	3.07	0.037(2)	0.6639(1)	0.0136(9)	2.16(6)
	3.496	0.094(2)	0.6014(3)	0.0336(9)	1.33(7)
	3.941	0.202(2)	0.5174(11)	0.0780(14)	0.55(9)
$Q^{*2} = 2$	2.722	0.009(1)	0.7433(2)	0.0034(3)	3.42(9)
	3.195	0.036(2)	0.6825(1)	0.0125(1)	2.37(6)
	3.659	0.099(2)	0.6140(2)	0.0338(8)	1.39(9)
	4.072	0.199(3)	0.5367(9)	0.0722(21)	0.66(4)
$Q^{*2} = 3$	2.877	0.007(1)	0.7692(1)	0.0027(2)	3.90(15)
	3.393	0.035(3)	0.7038(4)	0.0113(11)	2.68(8)
	3.856	0.096(1)	0.6368(4)	0.0306(6)	1.61(8)
	4.318	0.210(5)	0.5520(9)	0.0713(26)	0.74(5)
$Q^{*2} = 4$	3.054	0.006(1)	0.7973(3)	0.0020(2)	4.55(27)
	3.642	0.035(2)	0.7254(2)	0.0105(6)	3.00(6)
	4.103	0.094(3)	0.6609(4)	0.0275(9)	1.92(18)
	4.6	0.216(3)	0.5738(8)	0.0675(20)	0.89(11)

$L^* = 0.4$	T^*	p^{S*}	$\rho^{*'}$	$\rho^{*''}$	γ^*
$Q^{*2} = 0$	1.893	0.005(0)	0.5807(6)	0.0030(1)	1.88(8)
	2.232	0.022(2)	0.5335(2)	0.0111(9)	1.31(7)
	2.536	0.055(2)	0.4836(2)	0.0274(10)	0.80(5)
	2.858	0.118(1)	0.4144(10)	0.0633(15)	0.33(5)
$Q^{*2} = 1$	1.925	0.005(1)	0.5866(2)	0.0029(5)	1.96(6)
	2.239	0.020(1)	0.5422(1)	0.0100(7)	1.39(6)
	2.573	0.055(2)	0.4873(2)	0.0270(13)	0.81(5)
	2.869	0.113(1)	0.4248(6)	0.0591(13)	0.37(4)
$Q^{*2} = 2$	1.999	0.005(1)	0.6004(4)	0.0026(4)	2.15(6)
	2.318	0.019(1)	0.5550(2)	0.0092(3)	1.53(4)
	2.663	0.056(2)	0.4983(4)	0.0262(13)	0.90(4)
	2.987	0.120(2)	0.4293(7)	0.0607(15)	0.37(3)
$Q^{*2} = 3$	2.096	0.004(0)	0.6193(4)	0.0021(3)	2.41(9)
	2.447	0.019(1)	0.5696(4)	0.0086(6)	1.69(14)
	2.794	0.056(1)	0.5130(3)	0.0245(7)	1.00(4)
	3.134	0.124(3)	0.4422(8)	0.0589(15)	0.43(2)
$Q^{*2} = 4$	2.213	0.003(1)	0.6395(4)	0.0016(3)	2.75(13)
	2.599	0.018(1)	0.5862(2)	0.0077(4)	1.87(10)
	2.972	0.057(2)	0.5268(4)	0.0235(11)	1.12(5)
	3.35	0.137(2)	0.4487(7)	0.0614(23)	0.45(3)

$L^* = 0.505$	T^*	p^{S*}	$\rho^{*'}$	$\rho^{*''}$	γ^*
$Q^{*2} = 0$	1.638	0.004(0)	0.5288(8)	0.0025(3)	1.57(5)
	1.913	0.015(1)	0.4888(3)	0.0087(4)	1.10(8)
	2.19	0.041(1)	0.4415(6)	0.0232(9)	0.67(4)
	2.476	0.091(1)	0.3774(10)	0.0571(7)	0.27(3)
$Q^{*2} = 1$	1.652	0.003(0)	0.5360(4)	0.0022(2)	1.65(4)
	1.924	0.014(1)	0.4954(11)	0.0079(3)	1.16(3)
	2.187	0.036(1)	0.4516(4)	0.0203(8)	0.75(6)
	2.509	0.092(1)	0.3806(9)	0.0558(11)	0.28(2)
$Q^{*2} = 2$	1.728	0.003(1)	0.5467(5)	0.0021(3)	1.77(8)
	2.029	0.016(1)	0.5015(1)	0.0087(5)	1.21(7)
	2.288	0.040(1)	0.4567(6)	0.0213(8)	0.76(6)
	2.584	0.091(1)	0.3913(9)	0.0530(13)	0.33(4)
$Q^{*2} = 3$	1.813	0.003(0)	0.5629(4)	0.0017(3)	1.99(7)
	2.102	0.013(1)	0.5196(8)	0.0069(5)	1.38(2)
	2.393	0.038(1)	0.4708(4)	0.0195(5)	0.86(5)
	2.692	0.091(1)	0.4068(4)	0.0494(15)	0.37(3)
$Q^{*2} = 4$	1.922	0.003(1)	0.5793(4)	0.0015(3)	2.22(11)
	2.252	0.014(1)	0.5311(2)	0.0069(5)	1.51(7)
	2.541	0.040(1)	0.4828(4)	0.0189(7)	0.96(6)
	2.885	0.102(3)	0.4090(5)	0.0525(24)	0.37(1)

$L^* = 0.6$	T^*	p^{S*}	$\rho^{*'}$	$\rho^{*''}$	γ^*
$Q^{*2} = 0$	1.475	0.003(1)	0.4892(3)	0.0022(5)	1.31(3)
	1.726	0.013(0)	0.4508(2)	0.0082(4)	0.92(5)
	1.948	0.031(1)	0.4111(3)	0.0199(7)	0.60(1)
	2.211	0.073(0)	0.3498(6)	0.0505(5)	0.24(2)
$Q^{*2} = 1$	1.49	0.003(0)	0.4958(3)	0.0020(3)	1.40(4)
	1.731	0.011(1)	0.4588(1)	0.0073(3)	1.01(4)
	2.011	0.036(2)	0.4084(3)	0.0224(13)	0.56(3)
	2.233	0.072(2)	0.3562(7)	0.0485(19)	0.27(3)
$Q^{*2} = 2$	1.552	0.003(0)	0.5070(3)	0.0019(2)	1.52(5)
	1.81	0.012(1)	0.4660(9)	0.0072(5)	1.05(6)
	2.08	0.036(1)	0.4177(3)	0.0213(5)	0.61(6)
	2.314	0.074(1)	0.3627(8)	0.0481(9)	0.28(2)
$Q^{*2} = 3$	1.61	0.002(0)	0.5248(3)	0.0013(2)	1.76(9)
	1.879	0.010(1)	0.4829(4)	0.0058(4)	1.21(5)
	2.137	0.030(1)	0.4378(3)	0.0167(4)	0.76(7)
	2.435	0.079(1)	0.3705(8)	0.0484(11)	0.30(5)
$Q^{*2} = 4$	1.725	0.002(0)	0.5372(1)	0.0012(2)	1.90(7)
	2.023	0.011(1)	0.4912(7)	0.0061(5)	1.29(5)
	2.284	0.033(1)	0.4460(4)	0.0173(9)	0.82(3)
	2.608	0.089(1)	0.3719(3)	0.0522(14)	0.29(3)

$L^* = 0.8$	T^*	p^{S*}	$\rho^{*'}$	$\rho^{*''}$	γ^*
$Q^{*2} = 0$	1.234	0.002(0)	0.4293(2)	0.0018(3)	1.03(2)
	1.426	0.008(0)	0.3968(6)	0.0062(3)	0.73(2)
	1.632	0.023(1)	0.3574(5)	0.0174(9)	0.44(3)
	1.856	0.055(1)	0.2993(2)	0.0464(16)	0.16(1)
$Q^{*2} = 1$	1.246	0.002(0)	0.4380(2)	0.0015(2)	1.11(4)
	1.458	0.008(1)	0.4020(6)	0.0060(5)	0.76(3)
	1.686	0.025(1)	0.3577(5)	0.0187(12)	0.44(2)
	1.885	0.055(1)	0.3061(10)	0.0448(9)	0.18(4)
$Q^{*2} = 2$	1.308	0.002(0)	0.4490(3)	0.0013(1)	1.21(5)
	1.514	0.007(0)	0.4138(5)	0.0055(2)	0.86(5)
	1.712	0.021(1)	0.3760(3)	0.0149(7)	0.54(4)
	1.933	0.051(1)	0.3220(4)	0.0388(10)	0.23(2)
$Q^{*2} = 3$	1.352	0.001(0)	0.4675(3)	0.0009(3)	1.39(11)
	1.579	0.006(1)	0.4296(4)	0.0043(6)	0.97(5)
	1.801	0.021(1)	0.3880(2)	0.0136(7)	0.61(6)
	2.045	0.055(1)	0.3290(7)	0.0394(6)	0.25(3)
$Q^{*2} = 4$	1.447	0.001(0)	0.4796(2)	0.0008(2)	1.54(8)
	1.674	0.006(1)	0.4430(3)	0.0039(4)	1.09(3)
	1.914	0.021(1)	0.3992(2)	0.0130(7)	0.68(1)
	2.187	0.060(1)	0.3338(3)	0.0406(10)	0.25(1)

Table 3: Fit parameters for A^* from Eq. (9), correlated to the present simulation results.

a_1	1.81404	d_2	1.15865
		d_3	$-7.74845 \cdot 10^{-1}$
b_1	$1.43624 \cdot 10^{-1}$		
b_2	$-3.66120 \cdot 10^{-1}$	e_2	$6.38307 \cdot 10^{-2}$
b_3	$9.70532 \cdot 10^{-3}$	e_5	$1.66285 \cdot 10^{-2}$
c_1	1.03576		

Table 4: Fit parameters for P^* from Eq. (12), correlated to the present simulation results.

α_1	1.80157
β_1	$2.55606 \cdot 10^{-1}$
β_2	1.39008
β_3	-1.05375